*Journal for Multiscale Computational Engineering*, 10 (1): 13–31 (2012)

# COARSE GRAINING OF ATOMISTIC DESCRIPTION AT FINITE TEMPERATURE USING FORMAL ASYMPTOTICS

***Yashashree Kulkarni***

*Department of Mechanical Engineering, University of Houston, Houston, TX 77204, E-mail: ykulkarni@uh.edu*

*In this paper, we propose a computational method for coarse graining the atomistic description at finite temperature using formal asymptotics. The method is based on the ansatz that there exists a separation of scales between the time scale of the atomic fluctuations and that of the thermodynamic processes, such as thermal expansion. We use the WKB method to propose an averaging scheme for treating the thermal degrees of freedom and deriving an effective Hamiltonian for the atomistic system. This energy functional is incorporated into the quasicontinuum framework to achieve a seamless coarse graining on the spatial scale. Numerical validation is performed by computing the thermal equilibrium properties of selected materials. The scope of the method based on the use of perturbation theory is discussed, and its capability is illustrated by way of simulating dislocation nucleation under a nanoindenter.*

**KEY WORDS:** *multiscale modeling, quasicontinnum method, WKB method, perturbation theory, thermal fluctuations*

## 1. INTRODUCTION

Advances in the fields of nanoscience and nanotechnology have led to a drive toward understanding material behavior and complex phenomena spanning multiple temporal and spatial scales. Consequently, the past decade has witnessed the development of several novel multiscale methods that aim to bridge the atomistic scales and the continuum description. These models are usually broadly classified as sequential or concurrent approaches. Sequential multiscale methods, such as E and Engquist (2003), Fish and Schwob (2003), Fish et al. (2007a), and Li et al. (2008), are top-down approaches in that the microscopic model is used to inform the macroscopic model whenever information from the fine scale is needed for the constitutive description. On the other hand, concurrent multiscale methods, such as Broughton et al. (1999), Rudd and Broughton (2005), Belytschko and Xiao (2003), and Fish et al. (2007b), simultaneously use different models in different regions of the domain and are distinct from other concurrent methods with regard to the models employed as well as the pathway of information exchange across the interface or the overlap region between the models. For comprehensive reviews, we refer the readers to Lu and Kaxiras (2005) and Curtin and Miller (2003). The focus of this work is on the quasicontinuum method, which is a concurrent multiscale approach for seamlessly bridging the atomistic and continuum realms.

The aim of this paper is the development of a finite temperature extension of the quasicontinuum (QC) method of Tadmor et al. (1996a,b). The static theory of the quasicontinuum furnishes a computational framework for seamlessly bridging the spatial length scales by allowing atomistic resolution in the regions of interest (i.e., in the vicinity of defects) and sequentially coarse graining the atomistic description in regions where the deformation field is slowly varying on the scale of the lattice. A number of finite-temperature multiscale methods based on QC have been proposed in the past within the framework of equilibrium statistical mechanics and thermodynamics [cf, e.g., Dupuy et al. (2005), Shenoy et al. (1999), Tang et al. (2006), and Wu et al. (2003)]. Recently, extensions to QC have also been developed for modeling nonequilibrium finite-temperature phenomena Kulkarni et al. (2008); Marian et al. (2010).

1543–1649/12/$35.00  

In this paper, we propose an alternative, computationally efficient approach toward coarse graining the atomistic dynamics using formal asymptotics. The QC extension proposed in this work is based on the fully three-dimensional version developed by Knap and Ortiz (2001).

The problem of ascertaining the thermodynamic behavior of materials as an averaged effect of the thermal fluctuations involves multiple scales in time. Thus, at nonzero temperatures, the problem of coarse graining is compounded by the hierarchy of temporal scales in addition to that of the spatial scales ranging from the atomistic to the continuum realms. We address this issue by first averaging over the thermal degrees of freedom using perturbation theory in order to obtain an effective thermodynamic potential that takes into account the effect of the thermal vibrations. The central idea is based on the ansatz that there exists a strict separation of scales between the time scale of the atomic fluctuations and that of the thermodynamic processes, such as thermal expansion and macroscopic deformation of the system. This enables us to regard the thermal oscillations of the atoms as perturbations about the slow macroscopic trajectory. To treat these atomic fluctuations, we use the WKB perturbation method, which is well-suited for asympotically approximating the solutions to linear ordinary differential equations (ODE), which exhibit high-frequency oscillations. As a consequence, the thermodynamic potentials obtained in this work are based on the local quasi-harmonic approximation, which has been shown by LeSar et al. (1989) to be reasonably accurate to at least half the melting temperature for moderately strained crystals.

For simplicity, we restrict attention to macroscopic processes that are quasi-static. We also assume the local equilibrium hypothesis. Under these conditions, the WKB method furnishes the internal energy of the system dependent on the positions and local temperatures associated with all the atoms. The problem of determining the stable equilibrium configurations of the system can then be stated as a problem of finding the *local* minima of this effective macroscopic energy. This structure greatly facilitates implementation, which is reduced to replacing ordinary interatomic potentials by temperature-dependent ones.

The paper is organized as follows: Section 2 provides an outline of the variational framework and the WKB method that form the basis of this work. The perturbation theory is then used to average over the thermal oscillations and derive the expression for the internal energy of the atomistic system. In Section 3, we discuss some properties and ramifications of using the WKB approximation to derive the effective Hamiltonian of the system. In Section 4, we invoke the Mie-Grüneisen approximation in order to further reduce the computational cost of computing the eigenfrequencies. Section 5 develops the finite-temperature framework of the quasicontinuum method using the WKB formulation. In Section 6, the results for some numerical validation tests are presented. Specifically, we calculate the thermal expansion for copper using the embedded-atom method potential and compare to experimental data and classical theory. A simulation of a dislocation punch-in under a nanoindenter is presented as an illustrative example. We conclude the paper by summarizing the limitations and the capabilities of the proposed method and discussing possible avenues for future method development in Section 7.

## 2. GENERAL FRAMEWORK

We consider a system with configuration space $Y \times X$. The states $(\boldsymbol{q}, \boldsymbol{u}) \in Y \times X$ of the system consist of macroscopic variables $\boldsymbol{u}$ and microscopic variables $\boldsymbol{q}$. We assume that the time scales of the variables are well separated, as illustrated in Fig. 1. That is,

$$\frac{\tau_u}{\tau_q} \gg 1 \tag{1}$$

where $\tau_u$ and $\tau_q$ are the average time periods of $\boldsymbol{u}$ and $\boldsymbol{q}$, respectively. For the sake of illustration, we consider a crystal at finite temperature with $N$ atoms occupying a subset $\mathscr{L}$ of a simple $d$-dimensional Bravais lattice. Without loss of generality, we shall consider a monatomic crystal. Denoting the basis vectors by $\{\boldsymbol{a}_i\,;\, i = 1, \dots d\}$, the reference coordinates of the atoms are

$$\boldsymbol{X}(\boldsymbol{l}) = \sum_{i=1}^{d} l^i \boldsymbol{a}_i, \quad \boldsymbol{l} \in Z \subset \mathbb{R}^d \tag{2}$$

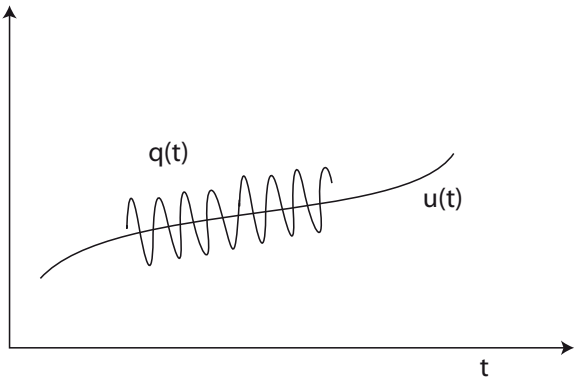


**FIG. 1:** Schematic representation of the microscopic and the macroscopic degrees of freedom

where $\boldsymbol{l}$ are the lattice coordinates associated with individual atoms, $Z$ is the set of integers, and $d$ is the dimension of space. We also normalize $\boldsymbol{u}$ and $\boldsymbol{q}$ with the mass of each atom

$$\boldsymbol{q}(\boldsymbol{l}) \to \frac{1}{\sqrt{m}}\,\boldsymbol{q}(\boldsymbol{l}), \quad \boldsymbol{u}(\boldsymbol{l}) \to \frac{1}{\sqrt{m}}\,\boldsymbol{u}(\boldsymbol{l}) \tag{3}$$

For notational convenience, $\boldsymbol{u}$ or $\boldsymbol{q}$ shall represent arrays of all the atomic displacements, whereas $\boldsymbol{u}(\boldsymbol{l})$ or $\boldsymbol{q}(\boldsymbol{l})$ shall refer to the corresponding displacement of atom $\boldsymbol{l}$. Let the displacement of each atom be decomposed into two components

$$\boldsymbol{u}(\boldsymbol{l}) + \boldsymbol{q}(\boldsymbol{l}) \tag{4}$$

where $\boldsymbol{u}(\boldsymbol{l})$ follows the macroscopic deformation of the crystal, and $\boldsymbol{q}(\boldsymbol{l})$ is the thermal oscillation of the atom. In this case,

$$X \equiv Y \equiv \mathbb{R}^{Nd} \tag{5}$$

Our aim is to derive an effective energy of the system, $E(\boldsymbol{u})$, accounting for the effect of the microscale fluctuations. To this end, we consider the Hamiltonian of the system

$$H(\boldsymbol{p}, \boldsymbol{q}, \boldsymbol{u}) = \frac{1}{2} \sum_{\boldsymbol{l} \in \mathscr{L}} |\boldsymbol{p}(\boldsymbol{l})|^2 + V(\boldsymbol{u}, \boldsymbol{q}) \tag{6}$$

where $\boldsymbol{p}(\boldsymbol{l})$ is the momentum associated with $\boldsymbol{q}(\boldsymbol{l})$ in the mass-reduced coordinates and $V(\boldsymbol{u}, \boldsymbol{q})$ is the potential energy of the system expressible through the use of empirical interatomic potentials. The inertial term due to $\boldsymbol{u}$ is neglected since $\boldsymbol{u}$ is quasistatic. According to statistical thermodynamics, the internal energy of the system is defined as the phase average of the Hamiltonian (Weiner, 2002). We shall assume ergodicity to express the internal energy as a time average

$$E(\boldsymbol{u}) = \lim_{T \to \infty} \frac{1}{T} \int_0^T H\left[\boldsymbol{p}(t), \boldsymbol{q}(t), \boldsymbol{u}(t)\right] dt \tag{7}$$

The energy is expressed as a function $E(\boldsymbol{u})$ based on the *ansatz* that the fluctuations satisfy, and hence can be determined from, their Euler-Lagrange equations

$$\ddot{\boldsymbol{q}} + \frac{\partial V}{\partial \boldsymbol{q}}\big(\boldsymbol{q}, \boldsymbol{u}\big) = 0 \tag{8}$$

We now wish to obtain a closed-form, albeit approximate, solution for $\boldsymbol{q}$ in terms of $\boldsymbol{u}$ by the use of perturbation theory. To this end, we first make the inherent separation of temporal scales explicit by introducing a sequence $(\boldsymbol{u}_\epsilon) \in \mathrm{X}$:

$$\boldsymbol{u}_\epsilon(t) = \boldsymbol{u}(\epsilon t); \;\; \epsilon \to 0 \tag{9}$$

$$E_\epsilon(\boldsymbol{u}) = \frac{\epsilon}{b}\int_0^{b/\epsilon} H\left[\boldsymbol{p}_\epsilon(t), \boldsymbol{q}_\epsilon(t), \boldsymbol{u}_\epsilon(t)\right] dt \tag{10a}$$

$$\text{with} \quad \ddot{\boldsymbol{q}}_\epsilon + \frac{\partial V}{\partial \boldsymbol{q}}\left(\boldsymbol{q}_\epsilon, \boldsymbol{u}_\epsilon\right) = 0 \tag{10b}$$

where we have replaced the time interval $[0, T]$ by $[0, b/\epsilon]$ with $\epsilon \to 0$ for the sake of simplicity. We wish to ascertain the behavior of the system as $\epsilon \to 0$. To this end, we first obtain the solution to Eq. (10b) by using perturbation theory, as described in Section 2.1. Substituting this approximate solution in Eq. (10a) and taking the limit $\epsilon \to 0$ yields the pointwise limit that we seek

$$E(\boldsymbol{u}) = \lim_{\epsilon \to 0} E_\epsilon(\boldsymbol{u}) \tag{11}$$

### 2.1 WKB Method

The WKB method is a singular perturbation method for obtaining approximate global solutions to *linear* differential equations whose highest derivative is multiplied by a small parameter, $\epsilon$. To reduce Eq. (10b) to such a form, we apply the following change of variables:

$$\tau = \epsilon t \tag{12}$$

Since $\epsilon$ is a small parameter, $\tau$ denotes a long time scale with respect to $t$. This yields

$$\epsilon^2 \frac{\partial^2 \boldsymbol{q}_\epsilon}{\partial \tau^2}(\tau) + \frac{\partial V}{\partial \boldsymbol{q}}[\boldsymbol{q}_\epsilon(\tau), \boldsymbol{u}(\tau)] = 0 \tag{13}$$

Because the WKB approach can be applied to systems of linear ODEs, it requires linearization of the equations of motion for $\boldsymbol{q}$. Hence, we assume in addition that $V$ possesses sufficient smoothness (i.e., $V \in C^2$) and appeal to the *local* quasi-harmonic approximation given by

$$V(\boldsymbol{q}_\epsilon, \boldsymbol{u}) \approx V(\boldsymbol{u}) + \frac{1}{2}\sum_{\boldsymbol{l} \in \mathscr{L}} \boldsymbol{q}_\epsilon^{\mathrm{T}}(\boldsymbol{l})\, \mathrm{K}(\boldsymbol{u}, \boldsymbol{l})\, \boldsymbol{q}_\epsilon(\boldsymbol{l}) \tag{14}$$

where $\mathrm{K}(\boldsymbol{u}, \boldsymbol{l})$ is the $d \times d$ dynamical matrix associated with the atom $\boldsymbol{l}$. The superscript $\mathrm{T}$ denotes a transpose. The local quasi-harmonic model has been proposed in the work of LeSar et al. (1989), in which it is shown to be reasonably accurate to at least half the melting temperature for moderately strained crystals. Substituting Eq. (14) into Eq. (10b) yields a system of linear differential equations for each atom

$$\epsilon^2(\boldsymbol{l})\boldsymbol{q}_\epsilon''(\boldsymbol{l}) + \mathrm{K}(\boldsymbol{u}, \boldsymbol{l})\, \boldsymbol{q}_\epsilon(\boldsymbol{l}) = 0\,; \;\; \forall \boldsymbol{l} \in \mathscr{L} \tag{15}$$

where $'$ denotes differentiation with respect to $\tau$. Applying the WKB method as described in Appendix A, we obtain the desired approximate expression for $\boldsymbol{q}_\epsilon(\boldsymbol{l})$ and the corresponding velocities

$$\boldsymbol{q}_\epsilon(\boldsymbol{l}, \tau) = \sum_j \frac{1}{\sqrt{\omega_j(\boldsymbol{u})}} \boldsymbol{v}_j(\boldsymbol{u}) \left\{ A_j \sin\left[\frac{1}{\epsilon}\int^\tau \omega_j(s)ds\right] + B_j \cos\left[\frac{1}{\epsilon}\int^\tau \omega_j(s)ds\right]\right\} \tag{16a}$$

$$\frac{d\boldsymbol{q}_\epsilon}{d\tau}(\boldsymbol{l}, \tau) = \frac{1}{\epsilon}\sum_j \sqrt{\omega_j(\boldsymbol{u})} v_j(\boldsymbol{u}) \left\{ A_j \cos\left[\frac{1}{\epsilon}\int^\tau \omega_j(s)ds\right] - B_j \sin\left[\frac{1}{\epsilon}\int^\tau \omega_j(s)ds\right]\right\} \tag{16b}$$

$A_i$ and $B_i$ are constants of integration that can be evaluated from the initial conditions.

## 2.2 Effective Temperature-Dependent Energy

We recall the family of energy functionals defined in Eq. (10a) and introduce the change of time variable from $t$ to $\tau = \epsilon t$

$$E_\epsilon(\boldsymbol{u}) = \frac{1}{b}\int_0^b H\left[\boldsymbol{p}_\epsilon(\tau), \boldsymbol{q}_\epsilon(\tau), \boldsymbol{u}(\tau)\right] d\tau \tag{17}$$

Under the quasi-harmonic approximation, the Hamiltonian in Eq. (6) has the form

$$H = \frac{1}{2}\sum_{\boldsymbol{l}\in\mathscr{L}} |\boldsymbol{p}_\epsilon(\boldsymbol{l})|^2 + V[\boldsymbol{u}(\tau)] + \frac{1}{2}\sum_{\boldsymbol{l}\in\mathscr{L}} \boldsymbol{q}_\epsilon^{\mathrm{T}}(\boldsymbol{l})\,\mathrm{K}(\boldsymbol{u},\boldsymbol{l})\,\boldsymbol{q}_\epsilon(\boldsymbol{l}) \tag{18}$$

Using the relation

$$\boldsymbol{p}_\epsilon(\boldsymbol{l}) = \dot{\boldsymbol{q}}_\epsilon(\boldsymbol{l}) = \epsilon\,\boldsymbol{q}'_\epsilon(\boldsymbol{l}),\ \ \forall\ \boldsymbol{l}\in\mathscr{L} \tag{19}$$

and substituting the solutions given in Eqs. (16a) and (16b) in the expression (18) simplifies the Hamiltonian to

$$H = V(\boldsymbol{u}) + \frac{1}{2}\sum_{\boldsymbol{l}\in\mathscr{L}}\sum_{i=1}^{d} \omega_i(\boldsymbol{u},\boldsymbol{l}) D_i^2(\boldsymbol{l}) \tag{20}$$

with

$$D_i^2(\boldsymbol{l}) = A_i^2(\boldsymbol{l}) + B_i^2(\boldsymbol{l}) \tag{21}$$

Finally, using Eq. (20) in expression (17) for the energy, we have

$$E_\epsilon(\boldsymbol{u}) = \frac{1}{b-a}\int_a^b \left[V(\boldsymbol{u}) + \frac{1}{2}\sum_{\boldsymbol{l}\in\mathscr{L}}\sum_{i=1}^{d} \omega_i(\boldsymbol{u},\boldsymbol{l}) D_i^2(\boldsymbol{l})\right] d\tau \tag{22}$$

We observe that $E_\epsilon(\boldsymbol{u})$ is independent of $\epsilon$. This implies that the right hand side of Eq. (22) is indeed the limit $E(\boldsymbol{u})$, and we have

$$E_\epsilon = E$$

for every $\boldsymbol{u} \in X$ and for $\epsilon \to 0$. Furthermore, we emphasize that since $\boldsymbol{u}$ is a quasistatic deformation, $\tau$ simply serves as an index for a continuous sequence of states at uniform thermodynamic equilibrium. Interpreted as time, $\tau$ represents an arbitrary slow process on the macroscopic time scale. Hence, we can rewrite the internal energy as

$$E(\boldsymbol{u}) = V(\boldsymbol{u}) + \frac{1}{2}\sum_{\boldsymbol{l}\in\mathscr{L}}\sum_{i=1}^{d} \omega_i(\boldsymbol{u},\boldsymbol{l}) D_i^2(\boldsymbol{l}) \tag{23}$$

### *2.2.1 Determination of $D_i(\boldsymbol{l})$*

In molecular dynamics, the equilibrium temperature is prescribed and maintained through the atomic velocities, based on the equipartition of energy. We follow the same procedure in order to express the dependence of $E(\boldsymbol{u})$ on the local temperature through the $D_i(\boldsymbol{l})$. To this end, we invoke the local equilibrium hypothesis and introduce the notion of a local temperature, $T(\boldsymbol{l})$, associated with each atom. We let the initial configuration of the system be an equilibrium state at zero temperature.

$$\boldsymbol{u}(\boldsymbol{l})|_{\tau=0} = \boldsymbol{u}_0(\boldsymbol{l}) \tag{24a}$$

$$\boldsymbol{q}_\epsilon(\boldsymbol{l})|_{\tau=0} = \boldsymbol{q}_0(\boldsymbol{l}) \tag{24b}$$

$$\dot{\boldsymbol{q}}_\epsilon(\boldsymbol{l})|_{\tau=0} = \epsilon\,\boldsymbol{q}'_\epsilon(\boldsymbol{l})|_{\tau=0} = \mathbf{v}_0(\boldsymbol{l}) \tag{24c}$$

Substituting Eqs. (24a)–(24c) into Eqs. (16a)–(16b) at $\tau = 0$, the $A_i(\boldsymbol{l})$ and $B_i(\boldsymbol{l})$ are determined as

$$B_i(\boldsymbol{l}) = \sqrt{\omega_i(\boldsymbol{u}_0,\boldsymbol{l})}\ \left[\boldsymbol{v}_i^{\mathrm{T}}(\boldsymbol{u}_0,\boldsymbol{l})\,\boldsymbol{q}_0(\boldsymbol{l})\right],\ \ i = 1,\ldots d \tag{25a}$$

$$A_i(\boldsymbol{l}) = \frac{1}{\sqrt{\omega_i(\boldsymbol{u}_0, \boldsymbol{l})}} \left[\boldsymbol{v}_i^{\mathrm{T}}(\boldsymbol{u}_0, \boldsymbol{l})\, \mathbf{v}_0(\boldsymbol{l})\right], \;\; i = 1, \ldots d \tag{25b}$$

where we have exploited the orthogonality of the eigenvectors $\boldsymbol{v}(\boldsymbol{l})$. Writing $\mathbf{v}_0(\boldsymbol{l})$ and $\boldsymbol{q}_0(\boldsymbol{l})$ in the principal coordinates

$$\mathbf{v}_0(\boldsymbol{l}) = \sum_{i=1}^{d} \boldsymbol{v}_i(\boldsymbol{u}_0, \boldsymbol{l}) V_i(\boldsymbol{l}), \;\; \boldsymbol{q}_0(\boldsymbol{l}) = \sum_{i=1}^{d} \boldsymbol{v}_i(\boldsymbol{u}_0, \boldsymbol{l}) Q_i(\boldsymbol{l}) \tag{26}$$

we have

$$D_i^2(\boldsymbol{l}) = \frac{1}{\omega_i(\boldsymbol{u}_0, \boldsymbol{l})}[V_i^2(\boldsymbol{l}) + \omega_i^2(\boldsymbol{u}_0, \boldsymbol{l}) Q_i^2(\boldsymbol{l})] \tag{27}$$

Assuming local equilibrium, we appeal again to the equipartition theorem to yield

$$\frac{1}{2}[V_i^2(\boldsymbol{l}) + \omega_i^2(\boldsymbol{u}_0, \boldsymbol{l}) Q_i^2(\boldsymbol{l})] = k_B T_0(\boldsymbol{l}), \;\; i = 1, \ldots d \tag{28}$$

which in turn gives

$$D_i^2(\boldsymbol{l}) = 2\frac{k_B T_0(\boldsymbol{l})}{\omega_i(\boldsymbol{u}_0, \boldsymbol{l})} \tag{29}$$

$T_0(\boldsymbol{l})$ is the initial prescribed temperature. Thus, the internal energy of the system, given in (23), becomes

$$E(\boldsymbol{u}) = V(\boldsymbol{u}) + \sum_{\boldsymbol{l} \in \mathscr{L}} k_B T_0(\boldsymbol{l}) \sum_{i=1}^{d} \frac{\omega_i(\boldsymbol{u}, \boldsymbol{l})}{\omega_i(\boldsymbol{u}_0, \boldsymbol{l})} \tag{30}$$

An important remark in place here is that $E(\boldsymbol{u})$ is the internal energy of a system, which need not be in thermal equilibrium. In other words, the system may have different temperatures in different regions and should only satisfy the local thermal equilibrium hypothesis, which enables us to define a local temperature, $T(\boldsymbol{l})$.

## 3. ADIABATIC INVARIANCE

In this section, we seek to understand some properties of the effective energy derived in the previous section based on its structure as given in Eq. (30). We note that the effective Hamiltonian obtained by formal asymptotics without the *local* quasi-harmonic approximation (i.e., by using the $Nd \times Nd$ global stiffness matrix of the system) is

$$H(\boldsymbol{u}) = V(\boldsymbol{u}) + \frac{1}{2}\sum_{i=1}^{Nd} D_i^2 \omega_i(\boldsymbol{u}) \tag{31}$$

This result is identical to the effective potential derived in the work of Bornemann (1998) on the homogenization in time of singularly perturbed mechanical systems. A model problem used in this study is a conservative dynamical system, with the displacement having a very fast and a slow component and a constraining potential having a quadratic form. Unlike our approach, this work uses the method of weak convergence in order to determine a homogenized potential energy for the limiting mechanical system on the continuum scale. For details of the analysis, we refer the reader to Bornemann (1998).

We now show that the internal energy given by Eq. (30) describes a system undergoing an adiabatic process, and hence, the problem of finding the metastable equilibrium configurations of the system can be enunciated as a minimization problem

$$\inf_{\boldsymbol{u} \in \mathrm{X}} E(\boldsymbol{u}) \tag{32}$$

We refer to the work of Bornemann (1998) and present some physical arguments in support of our claim. We first observe that the internal energy in Eq. (30) is a function of only one state variable, which is the deformation of the system. Thus, the only two ways of changing the total energy of the system are by either prescribing a different initial

temperature or by deforming it. This implies that the minimization problem stated in Eq. (32) describes a system subjected to mechanical deformation under adiabatic conditions. This is in agreement with classical thermodynamics in that the isentropic processes are modeled by minimizing the internal energy. In the absence of entropy sources or sinks within the system, adiabatic and isentropic conditions are equivalent.

This is also verified by the following calculations relating the current and the initial temperature distribution within the system. For any system, the internal energy calculated using the harmonic approximation comprises of the interatomic potential $V(\boldsymbol{u})$, which may be anharmonic, and the energy contained in the thermal oscillations of the atoms, which is harmonic by assumption. If the system is in local thermal equilibrium,

$$E(\boldsymbol{u}) = V(\boldsymbol{u}) + \sum_{\boldsymbol{l}\in\mathscr{L}} d\, k_B T(\boldsymbol{l}) \tag{33}$$

$T(\boldsymbol{l})$ being the current local temperature. Comparing Eqs. (33) and (30), we have

$$d\, T(\boldsymbol{l}) = T_0(\boldsymbol{l}) \sum_{i=1}^{d} \frac{\omega_i(\boldsymbol{u},\boldsymbol{l})}{\omega_i(\boldsymbol{u}_0,\boldsymbol{l})} \tag{34}$$

Because the equipartition of energy implies equal distribution of the energy among all modes, we get

$$T(\boldsymbol{l}) = T_0(\boldsymbol{l}) \frac{\omega_i(\boldsymbol{u},\boldsymbol{l})}{\omega_i(\boldsymbol{u}_0,\boldsymbol{l})},\ \forall i = 1,\ldots,d \tag{35}$$

It is evident that the temperature of the system changes only when there is a change in the mechanical configuration of the system. Therefore, Eq. (35) describes the evolution of local temperature during an adiabatic process. This relation can also be derived rigorously based on the adiabatic invariance of the normal action proved in Bornemann (1998). For a dynamical system whose effective potential is given by Eq. (31), the normal action is defined as the energy-frequency ratio

$$\theta^i_\epsilon = \frac{E^i_\epsilon}{\omega_i(\boldsymbol{u})} \tag{36}$$

$E^i_\epsilon$ is the energy of the $i$th mode. By way of weak convergence, it is shown that

$$\theta^i_\epsilon \rightharpoonup \theta^i_0 = \text{const} \tag{37}$$

This is known as the adiabatic invariance of the normal action. Applying this to our problem, we obtain the local relation

$$\frac{k_B T(\boldsymbol{l})}{\omega_i(\boldsymbol{u},\boldsymbol{l})} = \text{const} \tag{38}$$

which is the same as Eq. (35).

## 4. MIE-GRÜNEISEN APPROXIMATION

The expression for energy furnished by Eq. (30) requires the computation of frequencies associated with each atom. In addition, the computation of forces in the associated minimization problem involves derivatives of the frequencies with respect to $\boldsymbol{u}$, which can be achieved only by numerical differentiation. We circumvent these requirements by appealing to the Mie-Grüneisen approximation as shown below.

**Claim 1.** *Consider a system in local thermal equilibrium with $\omega_i(\boldsymbol{u},\boldsymbol{l})$ being the phonon frequencies associated with atom $\boldsymbol{l}$. Then, under the Mie-Grüneisen approximation applied locally*

$$\frac{\omega_i(\boldsymbol{u},\boldsymbol{l})}{\omega_i(\boldsymbol{u}_0,\boldsymbol{l})} = \text{const},\ \ i = 1,\ldots,d \tag{39}$$

*Proof.* The Mie-Grüneisen approximation states that, for a system in thermal equilibrium, the Grüneisen parameter, defined as

$$\gamma(V) = -\left(\frac{\partial \ln \omega_i}{\partial \ln V}\right)_T, \ i = 1, \ldots, Nd \tag{40}$$

is the same for all modes. The implication of this approximation is that the phonon frequencies are not functions of the equilibrium temperature explicitly but depend on it through the volume, $V$. As we noted earlier, the system under consideration needs only to be in local thermal equilibrium. Hence, we apply the Mie-Grüneisen approximation locally, the Grüneisen parameter for each atom

$$\gamma(\boldsymbol{l}) = -\left[\frac{\partial \ln \omega_i(\boldsymbol{u}, \boldsymbol{l})}{\partial \ln V}\right]_{\boldsymbol{T}}, \ i = 1, \ldots, d \tag{41}$$

being the same for the $d$ modes of the atom. $\boldsymbol{T}$ represents an array of temperatures of all atoms. Thus, we do not impose $\gamma$ to be the same for all the atoms, although it may be same for atoms experiencing identical environments. Equation (41) can be simplified to

$$\gamma(\boldsymbol{l}) = -\left[\frac{V}{\omega_i(\boldsymbol{u}, \boldsymbol{l})} \frac{\partial \omega_i(\boldsymbol{u}, \boldsymbol{l})}{\partial \boldsymbol{u}} \cdot \frac{\partial \boldsymbol{u}}{\partial V}\right]_{\boldsymbol{T}} \tag{42}$$

By defining a new function $g_1(\boldsymbol{u}, \boldsymbol{l})$, we rewrite Eq. (42) as

$$\frac{\partial \omega_i(\boldsymbol{u}, \boldsymbol{l})}{\partial \boldsymbol{u}} = -\frac{\gamma(\boldsymbol{l})}{V} \frac{\partial V}{\partial \boldsymbol{u}} \omega_i(\boldsymbol{u}, \boldsymbol{l}) = g_1(\boldsymbol{u}, \boldsymbol{l}) \, \omega_i(\boldsymbol{u}, \boldsymbol{l}) \tag{43}$$

At the initial equilibrium configuration (i.e., when $\boldsymbol{u} = \boldsymbol{u}_0$)

$$\gamma_0(\boldsymbol{l}) = -\left.\frac{V_0}{\omega_i(\boldsymbol{u}_0, \boldsymbol{l})} \frac{\partial \boldsymbol{u}}{\partial V} \frac{\partial \omega_i(\boldsymbol{u}, \boldsymbol{l})}{\partial \boldsymbol{u}}\right|_0 \tag{44}$$

or

$$\left.\frac{\partial \omega_i(\boldsymbol{u}, \boldsymbol{l})}{\partial \boldsymbol{u}}\right|_0 = g_1(\boldsymbol{u}_0, \boldsymbol{l}) \, \omega_i(\boldsymbol{u}_0, \boldsymbol{l}) \tag{45}$$

Assuming sufficient smoothness of the function $g_1(\boldsymbol{u}, \boldsymbol{l})$, we compute the higher derivatives of the frequencies as follows:

$$\frac{\partial^2 \omega_i(\boldsymbol{u}, \boldsymbol{l})}{\partial \boldsymbol{u}^2} = g_1'(\boldsymbol{u}, \boldsymbol{l}) \, \omega_i(\boldsymbol{u}, \boldsymbol{l}) + g_1(\boldsymbol{u}, \boldsymbol{l}) \, \omega_i'(\boldsymbol{u}, \boldsymbol{l}) \tag{46a}$$

$$= [g_1'(\boldsymbol{u}, \boldsymbol{l}) + g_1^2(\boldsymbol{u}, \boldsymbol{l})]\omega_i(\boldsymbol{u}, \boldsymbol{l}) = g_2(\boldsymbol{u}, \boldsymbol{l}) \, \omega_i(\boldsymbol{u}, \boldsymbol{l}) \tag{46b}$$

where the prime denotes differentiation with respect to $\boldsymbol{u}$. Equation (46b) is obtained by substituting Eq. (43) into Eq. (46a). By similar calculations, we obtain a recursive expression for the $n^{th}$ derivative of $\omega_i(\boldsymbol{u}, \boldsymbol{l})$

$$\frac{\partial^n \omega_i(\boldsymbol{u}, \boldsymbol{l})}{\partial \boldsymbol{u}^n} = g_n(\boldsymbol{u}, \boldsymbol{l}) \, \omega_i(\boldsymbol{u}, \boldsymbol{l}) \tag{47}$$

with

$$g_n(\boldsymbol{u}, \boldsymbol{l}) = g_{n-1}'(\boldsymbol{u}, \boldsymbol{l}) + g_1(\boldsymbol{u}, \boldsymbol{l}) \, g_{n-1}(\boldsymbol{u}, \boldsymbol{l}), \ n \geq 2 \tag{48}$$

At the initial equilibrium configuration,

$$\left.\frac{\partial^n \omega_i(\boldsymbol{u}, \boldsymbol{l})}{\partial \boldsymbol{u}^n}\right|_0 = g_n(\boldsymbol{u}_0, \boldsymbol{l}) \, \omega_i(\boldsymbol{u}_0, \boldsymbol{l}), \ n \geq 1 \tag{49}$$

From Eq. (47), we observe that all derivatives of $\omega_i(\boldsymbol{u},\boldsymbol{l})$ are linear in $\omega_i(\boldsymbol{u},\boldsymbol{l})$. Assuming sufficient smoothness of $\omega_i(\boldsymbol{u},\boldsymbol{l})$, the $n$th-order Taylor series expansion for $\omega_i(\boldsymbol{u},\boldsymbol{l})$ about the initial equilibrium state is

$$\omega_i(\boldsymbol{u},\boldsymbol{l}) = \omega_i(\boldsymbol{u}_0,\boldsymbol{l}) + \left.\frac{\partial\omega_i(\boldsymbol{u},\boldsymbol{l})}{\partial\boldsymbol{u}}\right|_0 \cdot[\boldsymbol{u}-\boldsymbol{u}_0] + \frac{1}{2}\left.\frac{\partial^2\omega_i(\boldsymbol{u},\boldsymbol{l})}{\partial\boldsymbol{u}^2}\right|_0 [\boldsymbol{u}-\boldsymbol{u}_0]^2 + \cdots + \frac{1}{n!}\left.\frac{\partial^n\omega_i(\boldsymbol{u},\boldsymbol{l})}{\partial\boldsymbol{u}^n}\right|_0 [\boldsymbol{u}-\boldsymbol{u}_0]^n \quad (50)$$

Dividing throughout by $\omega_i(0)$ and using the expressions for the derivatives given in (49),

$$\frac{\omega_i(\boldsymbol{u},\boldsymbol{l})}{\omega_i(\boldsymbol{u}_0,\boldsymbol{l})} = 1 + g_1(\boldsymbol{u}_0,\boldsymbol{l})\boldsymbol{u} + \frac{1}{2}g_2(\boldsymbol{u}_0,\boldsymbol{l})\boldsymbol{u}^2 + \cdots + \frac{1}{n!}g_n(\boldsymbol{u}_0,\boldsymbol{l})\boldsymbol{u}^n \quad (51)$$

Because the right-hand side is independent of $i$, Eq. (51) shows that under the Mie-Grüneisen approximation, all frequencies of an atom change in the same ratio.

Thus, we may write

$$\frac{\omega_i(\boldsymbol{u},\boldsymbol{l})}{\omega_i(\boldsymbol{u}_0,\boldsymbol{l})} = \frac{a}{b}\,,\ \forall i = 1,\ldots,d \quad (52)$$

where $a/b$ is some constant. Furthermore, using the algebraic identity

$$\frac{a}{b} = \frac{c}{d} = \frac{a+c}{b+d} \quad (53)$$

we can write

$$\frac{\omega_i^2(\boldsymbol{u},\boldsymbol{l})}{\omega_i^2(\boldsymbol{u}_0,\boldsymbol{l})} = \frac{\sum_{i=1}^d \omega_i^2(\boldsymbol{u},\boldsymbol{l})}{\sum_{i=1}^d \omega_i^2(\boldsymbol{u}_0,\boldsymbol{l})} = \frac{\mathrm{TrK}(\boldsymbol{u},\boldsymbol{l})}{\mathrm{TrK}(\boldsymbol{u}_0,\boldsymbol{l})} \quad (54)$$

Consequently,

$$\sum_{i=1}^d \frac{\omega_i(\boldsymbol{u},\boldsymbol{l})}{\omega_i(\boldsymbol{u}_0,\boldsymbol{l})} = d\frac{a}{b} = d\sqrt{\frac{\mathrm{TrK}(\boldsymbol{u},\boldsymbol{l})}{\mathrm{TrK}(\boldsymbol{u}_0,\boldsymbol{l})}} \quad (55)$$

Thus, the internal energy attains the following form:

$$E(\boldsymbol{u}) = V(\boldsymbol{u}) + \sum_{\boldsymbol{l}\in\mathscr{L}} dk_B T_0(\boldsymbol{l})\sqrt{\frac{\mathrm{TrK}(\boldsymbol{u},\boldsymbol{l})}{\mathrm{TrK}(\boldsymbol{u}_0,\boldsymbol{l})}} \quad (56)$$

We use this expression for the internal energy in our subsequent calculations. An advantage of using Eq. (56) is that we can derive analytical expressions for the trace of the stiffness matrices and, hence, their derivatives with respect to $\boldsymbol{u}$. In addition, the use of traces and its derivatives improves the computational efficiency of the method as it eliminates the computation of the eigenvalues of the dynamical matrices. The expressions for the energy, forces, local stiffness matrices, and their derivatives for the EAM potentials are derived in Appendix B.

## 5. FINITE-TEMPERATURE QUASICONTINUUM METHOD

In this section, we review the formulation of the finite temperature quasicontinuum method on the basis of the results obtained in the previous sections. One of the merits of this approach is that it possesses the same structure as the zero temperature QC method, with the distinction that the energy functional to be minimized is not the potential energy but the effective energy furnished by the WKB method. Specifically, the energy functional is given by

$$\Phi(\boldsymbol{u}) = E(\boldsymbol{u}) + \Phi^{\mathrm{ext}}(\boldsymbol{u}) \quad (57)$$

where $E(\boldsymbol{u})$ is the internal energy given by Eq. (56), and $\Phi^{\mathrm{ext}}(\boldsymbol{u})$ is an external potential associated with the applied loads. Then, the problem of finding the set of minimizers of this energy functional may be stated as

$$\min_{\boldsymbol{u}\in X} \Phi(\boldsymbol{u}) \quad (58)$$

For systems with a very large number of atoms, this minimization problem presents a significant computational cost. The theory of the quasicontinuum provides a computational scheme for preserving the atomistic resolution in the regions of interest and treating atoms collectively where deformations are slow varying on the scale of the lattice.

We begin by replacing Eq. (58) by the constrained minimization of $\Phi(\boldsymbol{u})$ over a suitably chosen subspace $X_h$ of $X$. $X_h$ is constructed by selecting a reduced set $\mathscr{L}_h \subset \mathscr{L}$ of $N_h < N$ representative atoms or nodes based on the local variation in the deformation field. Introducing a triangulation $\mathscr{T}_h$ over $\mathscr{L}_h$, the macroscopic displacement, and the temperature of the remaining atoms are determined by piecewise linear interpolation of the nodal coordinates

$$\boldsymbol{u}_h(\boldsymbol{l}) = \sum_{\boldsymbol{l}_h \in \mathscr{L}_h} \varphi(\boldsymbol{l}|\boldsymbol{l}_h)\boldsymbol{u}_h(\boldsymbol{l}_h) \tag{59a}$$

$$T_h(\boldsymbol{l}) = \sum_{\boldsymbol{l}_h \in \mathscr{L}_h} \varphi(\boldsymbol{l}|\boldsymbol{l}_h)T_h(\boldsymbol{l}_h) \tag{59b}$$

where $\varphi(\boldsymbol{l}|\boldsymbol{l}_h)$ is the continuous and piecewise linear shape function associated with the representative atom, $\boldsymbol{l}_h \in \mathscr{L}_h$, evaluated at the point $\boldsymbol{X}(\boldsymbol{l})$. Its domain is restricted to the simplices $K \in \mathscr{T}_h$ incident on $\boldsymbol{l}_h$, and it satisfies

$$\varphi(\boldsymbol{l}'_h|\boldsymbol{l}_h) = \delta(\boldsymbol{l}'_h|\boldsymbol{l}_h) \tag{60a}$$

$$\sum_{\boldsymbol{l}_h \in \mathscr{L}_h} \varphi(\boldsymbol{l}|\boldsymbol{l}_h) = 1 \tag{60b}$$

where $\delta$ is the Dirac $\delta$ function. Equation (60b) ensures that a constant field is interpolated exactly by the basis functions. Using Eqs. (59a) and (59b) in the expression for $\Phi(\boldsymbol{u})$, taking variations with respect to the nodal variables $\boldsymbol{u}_h(\boldsymbol{l}_h)$, and enforcing stationarity yields the equilibrium equations. We follow the work of Knap and Ortiz (2001) to further reduce the cost of computing the full lattice sums involved in these expressions by introducing appropriate cluster summation rules. The final form for the effective equilibrium equations is obtained as

$$\sum_{\boldsymbol{l}'_h \in \mathscr{L}_h} n_h(\boldsymbol{l}'_h) \left[ \sum_{\boldsymbol{l} \in \mathscr{C}(\boldsymbol{l}'_h)} \boldsymbol{f}(\boldsymbol{l})\varphi(\boldsymbol{l}|\boldsymbol{l}_h) \right] = 0 \tag{61}$$

where $\mathscr{C}(\boldsymbol{l}_h)$ represents a cluster of lattice sites within a sphere of radius $r(\boldsymbol{l}_h)$ centered at the node $\boldsymbol{l}_h$. The cluster weights $n_h(\boldsymbol{l}_h)$ associated with the nodes, $\boldsymbol{l}_h \in \mathscr{L}_h$, are computed by requiring that the cluster summation rule be exact for all basis functions (Knap and Ortiz, 2001). The force at each site $\boldsymbol{l}$ is evaluated as

$$\boldsymbol{f}(\boldsymbol{l}) = \frac{\partial \Phi}{\partial \boldsymbol{u}(\boldsymbol{l})} \tag{62a}$$

$$= \frac{\partial E}{\partial \boldsymbol{u}(\boldsymbol{l})} + \frac{\partial \Phi^{\text{ext}}}{\partial \boldsymbol{u}(\boldsymbol{l})} \tag{62b}$$

with

$$\frac{\partial E}{\partial \boldsymbol{u}(\boldsymbol{l})} = \frac{\partial V}{\partial \boldsymbol{u}(\boldsymbol{l})} + \frac{d\, k_B}{2} \sum_{\boldsymbol{l}' \in \mathscr{L}} \left[ \frac{T_0(\boldsymbol{l})}{\sqrt{\text{TrK}(\boldsymbol{u}_0, \boldsymbol{l})\text{TrK}(\boldsymbol{u}, \boldsymbol{l})}} \frac{\partial}{\partial \boldsymbol{u}(\boldsymbol{l})} \text{TrK}(\boldsymbol{u}, \boldsymbol{l}') \right] \tag{63}$$

where $\boldsymbol{l}'$ denotes all the atoms in the neighborhood of atom $\boldsymbol{l}$ with a specified cutoff radius. As described in Section 3, the solutions to Eq. (58) yield the equilibrium configurations of the crystal under adiabatic conditions. Furthermore, in the absence of entropy sources within the body, this is equivalent to isentropic conditions. Consequently, if the entropy of the system remains constant during a process, the temperature of the system must change, because entropy and temperature are conjugate state variables. Therefore, after determining the new equilibrium state of the crystal by

solving Eq. (61), the new temperature distribution is obtained by evaluating the relation (35) at the nodes. Using the Mie–Grüneisen approximation, this relation becomes

$$T_h(\boldsymbol{l}_h) = T_0(\boldsymbol{l}_h)\sqrt{\frac{\mathrm{TrK}(\boldsymbol{u}, \boldsymbol{l}_h)}{\mathrm{TrK}(\boldsymbol{u}_0, \boldsymbol{l}_h)}} \tag{64}$$

Finally, the flexibility of the quasicontinuum method is further enhanced by the use of adaptive mesh refinement in order to tailor the computational mesh to the structure of the deformation field. We again refer the readers to the work of Knap and Ortiz (2001) for a detailed discussion of the adaption indicator used in the current work.

## 6. NUMERICAL VALIDATION AND TESTS

In this section, we present our calculations for the thermal expansion of materials and a simulation of dislocation nucleation and propagation under a nanoindenter. The samples used in our simulations are face-centered cubic (fcc) crystals with the crystallographic orientation as shown in Fig. 2. It bears emphasis that the choice of materials is dictated by our choice of empirical interaction potentials for fcc crystals, namely, the Lennard-Jones pair potential and the EAM potential for Copper developed by Johnson (1988). The proposed method is general enough to be applied to any crystal structure and interatomic potentials.

### 6.1 Thermal Expansion

The sample used for these tests is a cube of an fcc crystal consisting of 108 atoms with periodic boundary conditions. The crystal is assumed to be perfect, and only the first nearest-neighbor interactions are considered. Since the crystal, subjected to a uniform temperature, undergoes a uniform thermal expansion, we use the change in lattice parameter as the only mechanical degree of freedom for the whole system. Thus, the energy minimization problem is reduced to

$$\min_a \Phi \tag{65}$$

where $a$ is the lattice parameter. The sample is prescribed a uniform temperature $T_0$ and is equilibrated by solving the minimization problem (65) using the conjugate gradient method. Because our approach assumes adiabatic conditions, the temperature of a system must change during the process. The uniform temperature of the system in the deformed configuration is evaluated as

$$T = T_0\sqrt{\frac{\mathrm{TrK}(a, b)}{\mathrm{TrK}(a_0, b)}} \tag{66}$$

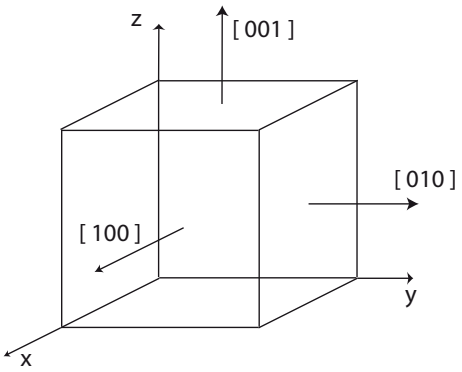


**FIG. 2:** Crystallographic orientation of the test sample used in the simulations

where $a$ and $a_0$ denote the current and initial lattice constants, and $b$ denotes an atom in the crystal. This computation is performed after the system achieves equilibrium at the prescribed temperature, and this value of $T$ is used in plotting the thermal expansion versus temperature. Figure 3 shows the thermal expansion of Cu versus temperature based on the EAM-Johnson potential. The plots compare the results for the WKB approach with experimental data (Niz and MacNair, 1941) as well as the classical results based on the quasi-harmonic approximation. It is instructive to note that the results of the WKB approach obtained for adiabatic conditions are identical to the classical results that are obtained for isothermal conditions. This demonstrates the equivalence of the ensembles in the thermodynamic limit (Zubarev, 1974), i.e., when the number of particles in the system is very large, the microcanonical and the canonical ensemble yield the same thermodynamic functions. Moreover, as expected, the results for the WKB method and the classical results have a linear dependence on temperature and are in good agreement with the experimental results up to about half the melting point of Cu. This is also in agreement with the results of LeSar et al. (1989).

## 6.2 Dislocation Nucleation under a Nanoindenter

As a concluding illustrative example, we present the simulation of the microstructural evolution via defect nucleation and propagation under a nanoindenter. We use this example to demonstrate the capabilities of the proposed method and open directions for future applications.

### *6.2.1 Test Problem Definition*

The test sample is an fcc nearest-neighbor Lennard-Jones crystal with $32 \times 32 \times 32$ unit cells, or a total of 137,313 atoms. The surfaces of the sample are aligned with the cube directions (Fig. 2). The imposed boundary conditions are prescribed in order to allow stress-free initial thermal expansion of the crystal. The indenter is applied on this relaxed sample. An initial temperature of $0.5T_m$ is prescribed, and all the surfaces are thermally insulated. The initial mesh is tailored to have atomistic resolution just under the indenter and an increasingly coarser triangulation away from this region. Figure 4 shows the triangulation of a cross section through the center of the cube with $x =$ const. The initial number of nodes is 757, which is a significant reduction from the total number of atoms.

As proposed by Kelchner et al. (1998), the spherical indenter is implemented as an external potential interacting with atoms on the top surface of the cube. The potential is of the form

$$\Phi^{\text{ext}}(r) = A\,H(R-r)\,(R-r)^3 \tag{67}$$

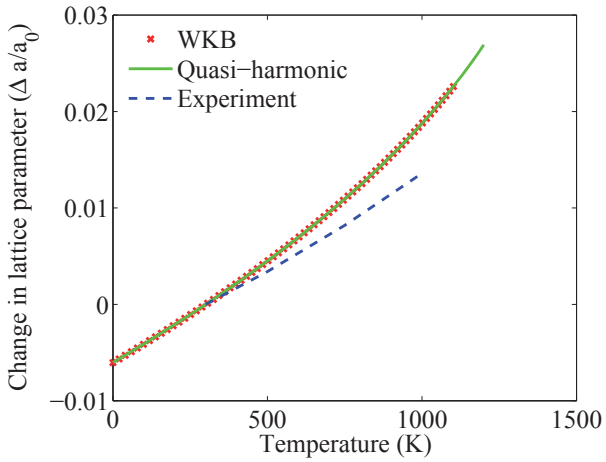


**FIG. 3:** Thermal expansion of a perfect crystal of Cu. The results are based on the EAM-Johnson potential.

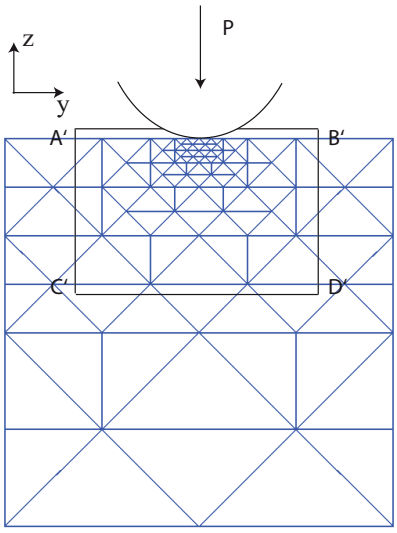


**FIG. 4:** Geometry of the nanoindentation setup for a spherical indenter and the initial mesh. A′B′C′D′ is the region shown in the snapshots of the temperature evolution.

where $R$ is the radius of the indenter, $r$ is the distance between a site and the center of the indenter, $A$ is a force constant, and $H(r)$ is the step function. In our calculations, the parameters have the following values:

$$R = 25[\sigma], \quad A = 2000\left[\frac{4\epsilon}{\sigma^3}\right] \tag{68}$$

where σ and ϵ are the parameters in the Lennard-Jones potential that set the energy and length scales, respectively.

### *6.2.2 Discussion*

Figures 5 and 6 show the snapshots of the temperature profile in the vicinity of the indenter at various indenter depths during the simulation. The images are of the region A'B'C'D' of the cross-section under the indenter, shown schematically in Fig. 4. Figure 7 also shows a comparison of the force versus indenter depth curves obtained at finite temperature and zero temperature. These results lead to the following qualitative interpretations. Figures 5 and 6 show a significant change in temperature during the simulation. Although the prescribed temperature is $0.5\,T_m$, the temperature at the start of indentation is about $0.32\,T_m$ because the initial thermal expansion is adiabatic. The maximum temperature reached when $\delta = -1.8\,[\sigma]$ is about $0.58\,T_m$, which is a 80% rise. This may be an implication of the quasi-harmonic approximation, which is found to give higher estimates for thermal expansion. Consequently, it should also predict greater change in the local temperatures, which depend on the local deformation through Eq. (61). Our simulation also confirms that defects are nucleated earlier at finite temperature, which is in qualitative agreement with the observation of Dupuy et al. (2005) and the experimental study by Schuh et al. (2005). The difference in the images at $\delta = -1.4\,[\sigma]$ and $\delta = -1.5\,[\sigma]$ shows that the dislocation nucleation leads to an increase in temperature under the indenter along the (111) slip plane. On continuing the loading (Fig. 6), the dislocation is observed to move toward the free surface, while the hot region under the indenter along the slip plane continues to spread. Figure 8 shows the dislocation structure under a spherical indenter predicted by our method and extracted using the centrosymmetry parameter (Kelchner et al., 1998). The result is in agreement with defect structures observed in fcc crystals (Hull and Bacon, 2001). A partial dislocation loop is nucleated under the indenter along the (111) plane. We do not see the trailing partial as the stacking fault grows in area with further indentation.

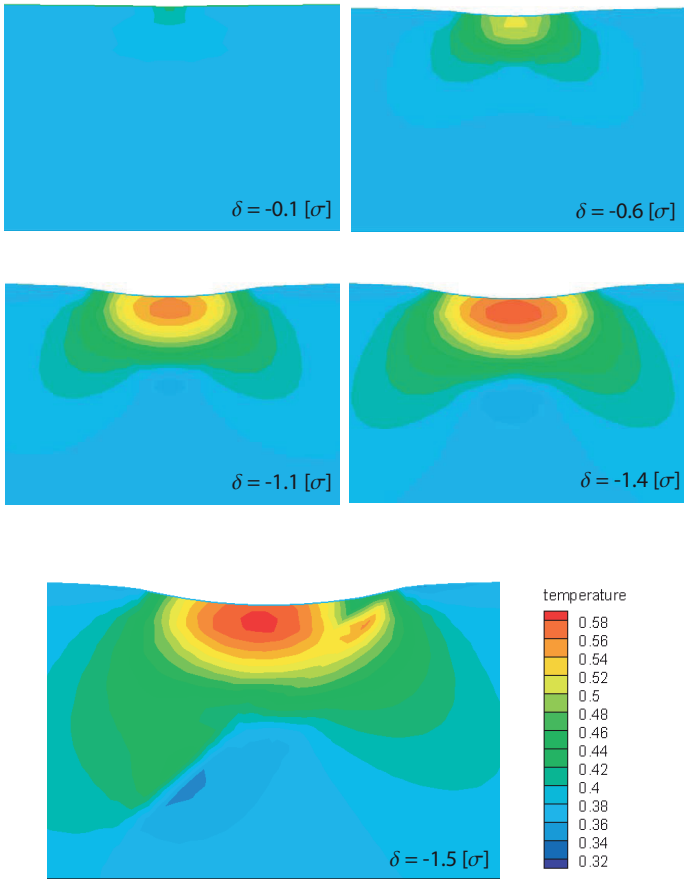


**FIG. 5:** Snapshots showing the temperature profile of a section under the indenter at different indentation depths during the simulation

## 7. CONCLUDING REMARKS

In this paper, we have developed a computational method for coarse graining the atomistic dynamics at finite temperature. This is accomplished by way of systematically averaging the thermal vibrations of the atoms using the WKB perturbation theory. To this end, we assume a strict separation of scales between the time scale of the thermal fluctuations and the macroscopic processes, such as thermal expansion or quasistatic deformation of the system. By treating the thermal vibrations as perturbations about the macroscopic trajectory, the WKB method yields an effective internal energy for the atomistic system. The local equilibrium hypothesis yields a local form for the energy functional dependent on the mean position and local temperature of all atoms and also allows for nonuniform temperature through the system. This approximation scheme is then taken as the basis for developing a finite-temperature extension of the QC method.

The main advantage of this multiscale approach is that it allows for a seamless bridging of the atomistic and continuum realms at finite temperature, with atomistic resolution only in the region of interest. Because the thermal degrees of freedom are accounted for in the energy functional, the method is not limited by the time scale of the atomic oscillations, which is one of the severe limitations of other molecular dynamics-based methods. In the spirit of the QC theory, the method requires only an interatomic potential as the sole empirical input and is capable of capturing the microstructural evolution and the associated thermomechanical behavior, albeit under adiabatic conditions. Moreover, the Mie-Grüneisen approximation simplifies the numerical implementation of the method and further reduces the

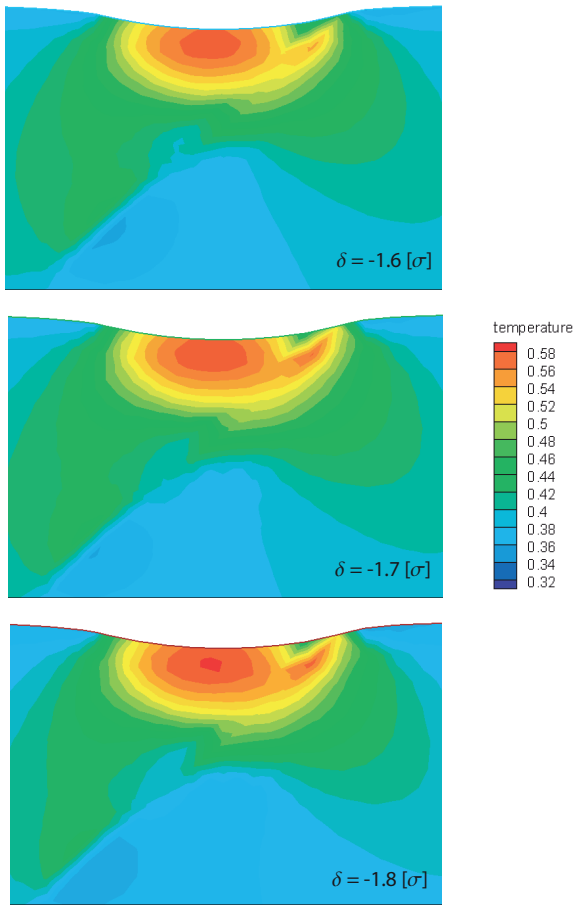


**FIG. 6:** Snapshots at subsequent load increments showing the temperature profile under the indenter after a dislocation has nucleated

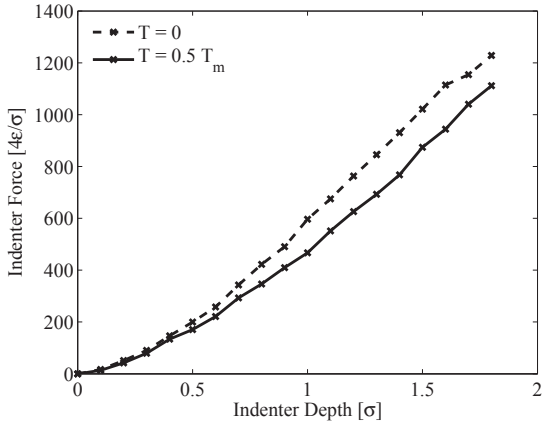


**FIG. 7:** Force vs. indenter depth plot for the simulation of a spherical indenter on a LJ fcc crystal using the WKB method.

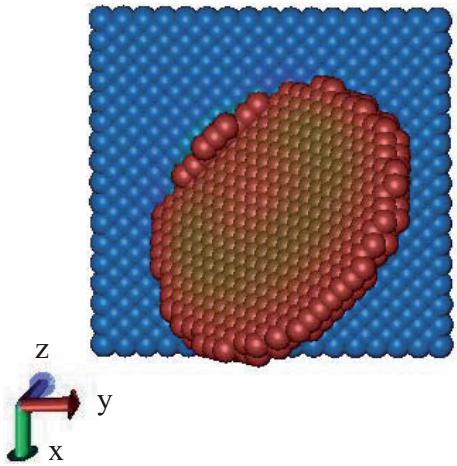


**FIG. 8:** Dislocation structure under a spherical indenter. The image shows the energetic atoms under the top surface of the crystal.

computational cost of evaluating the eigenfrequencies of the system. However, one of the limitations of this approach is that it relies on the local quasi-harmonic approximation and is restricted to temperatures only up to half the melting temperature of materials. Nevertheless, it is worth noting that the numerical results for thermal expansion based on the WKB approach are in excellent agreement with the classical results based on the quasi-harmonic approximation. Another important aspect of this method is that it is suitable only for locally adiabatic conditions and hence does not support heat transport through the system. Finally, following the work of Bornemann (1998), we note that a possible avenue for future work is the development of a dynamic version of the finite temperature QC method. This would be based on the effective Hamiltonian for the macroscopic dynamic system furnished by the WKB method or by weak convergence as shown in Bornemann (1998).

## ACKNOWLEDGMENTS

The work presented in this paper was performed as part of the author's doctoral work at Caltech under the supervision of Professor Michael Ortiz. The author also acknowledges the support of the Defense Advanced Research Projects Agency under the grant N66001-10-1-4033.

## REFERENCES

Belytschko, T. and Xiao, S., Coupling methods for continuum models with molecular models, *Int. J. Multiscale Comput. Eng.*, vol. **1**, pp. 115–126, 2003.

Bender, C. M. and Orszag, S. A., *Advanced Mathematical Methods for Scientists and Engineers*, McGraw-Hill, New York, 1978.

Bornemann, F. A., *Homogenization in time of singularly perturbed mechanical systems*, Springer, 1998.

Broughton, J. Q., Abraham, F. F., Bernstein, N., and Kaxiras, E., Concurrent coupling of length scales: Methodology and application, *Phys. Rev. B*, vol. **60**, pp. 2391–2403, 1999.

Curtin, W. and Miller, R., Atomistic/continuum coupling in computational materials science, *Model. Simul. Mater. Sci. Eng.*, vol. **11**, pp. R33–R68, 2003.

Dupuy, L. M., Tadmor, E. B., Miller, R. E., and Phillips, R., Finite-temperature quasicontinuum: Molecular dynamics without all the atoms, *Phys. Rev. Lett.*, vol. **95**, pp. 060202–1–060202–4, 2005.

E, W. and Engquist, B., Heterogeneous multiscale methods, *Commun. Math. Sci.*, vol. **1**, pp. 87–132, 2003.

Fish, J., Chen, W., and Li, R., Generalized mathematical homogenization of atomistic media at finite temperatures in three dimensions, *Comput. Methods Appl. Mech. Eng.*, vol. **196**, pp. 908–922, 2007a.

Fish, J., Nuggehally, M. A., Shephard, M. S., Picu, C. R., Badia, S., Parks, M. L., and Gunzburger, M., Concurrent atc coupling based on a blend of the continuum stress and the atomistic force, *Comput. Methods Appl. Mech. Eng.*, vol. **196**, pp. 4548–4560, 2007b.

Fish, J. and Schwob, C., Constitutive modeling based on atomistics, *Int. J. Multiscale Comput. Eng.*, vol. **1**, pp. 43–56, 2003.

Hull, D. and Bacon, D. J., *Introduction to Dislocations*, Butterworth-Heinemann, Oxford, 2001.

Johnson, R. A., Analytic nearest-neighbor model for fcc metals, *Phys. Rev. B*, vol. **37**, pp. 3924–3931, 1988.

Kelchner, C. L., Plimpton, S. J., and Hamilton, J. C., Dislocation nucleation and defect structure during surface nanoindentation, *Phys. Rev. B*, vol. **58**, pp. 11085–11088, 1998.

Knap, J. and Ortiz, M., Ananalysis of the quasicontinuum method, *J. Mech. Phys. Solids*, vol. **49**, pp. 1899–1923, 2001.

Kulkarni, Y., Knap, J., and Ortiz, M., A variational approach to coarse graining of equilibrium and non-equilibrium atomistic description at finite temperature, *J. Mech. Phys. Solids*, vol. **56**, pp. 1417–1449, 2008.

LeSar, R., Najafabadi, R., and Srolovitz, D., Finite-temperature defect properties from free-energy minimization, *Phys. Rev. Letters*, vol. **63**, pp. 624–627, 1989.

Li, A., Li, R., and Fish, J., Generalized mathematical homogenization: From theory to practice, *Comput. Methods Appl. Mech. Eng.*, vol. **197**, pp. 3225–3248, 2008.

Lu, G. and Kaxiras, K., An overview of multiscale simulations of materials, *Handbook of Theoretical and Computational Nanotechnology*, American Scientific, Stevenson Ranch, CA, 2005.

Marian, J., Venturini, G., Hansen, B., Knap, J., Ortiz, M., and Campbell, G., Finite-temperature extension of the quasicontinuum method using langevin dynamics: Entropy losses and analysis of errors, *Modell. Simul. Mater. Sci. Eng.*, vol. **18**, pp. 015003–1–31, 2010.

Nix, F. C. and MacNair, D., The thermal expansion of pure metals: Copper, gold, aluminum, nickel and iron, *Phys. Rev.*, vol. **60**, pp. 597–605, 1941.

Rudd, R. E. and Broughton, J. Q., Coarse-grained molecular dynamics: Nonlinear finite elements and finite temperature, *Phys. Rev. B*, vol. **72**, pp. 144104–1–144104–32, 2005.

Schuh, C. A., Mason, J. K., and Lund, A. C., Quantitative insight into dislocation nucleation from high-temperature nanoindentation experiments, *Nat. Mater.*, vol. **4**, pp. 617–621, 2005.

Shenoy, V., Shenoy, V., and Phillips, R., Finite temperature quasicontinuum methods, *Mater. Res. Soc. Symp. Proc.*, vol. **538**, pp. 465–471, 1999.

Tadmor, E. B., Ortiz, M., and Phillips, R., Quasi continuum analysis of defects in solids, *Philos. Mag. A*, vol. **73**, pp. 1529–1563, 1996.

Tadmor, E. B., Phillips, R., and Ortiz, M., Mixed atomistic and continuum models of deformation in solids, *Langmuir*, vol. **12**, pp. 4529–4534,1996.

Tang, Z., Zhao, H., Li, G., and Aluru, N. R., Finite-temperature quasicontinuum method for multiscale analysis of silicon nanostructures, *Phys. Rev. B*, vol. **74**, pp. 064110–1–064110–16, 2006.

Weiner, J. H., *Statistical Mechanics of Elasticity*, Dover, 2002.

Wu, Z. B., Diestler, D. J., Feng, R., and Zeng, X. C., Coarse-graining description of solid systems at nonzero temperature, *J. Chem. Phys.*, vol. **119**, pp. 8013–8023, 2003.

Zubarev, D. N., *Non-Equilibrium Statistical Thermodynamics*, Consultants Bureau, New York, 1974.

## APPENDIX A: WKB APPROXIMATION

The WKB method is a perturbation technique for obtaining approximate global solutions to linear differential equations whose highest derivative is multiplied by a small parameter $\epsilon$. The WKB approximation for such singularly perturbed problems is illustrated using the following example from Bender and Orszag (1978). Consider the ODE

$$\epsilon^2 \ddot{y}(t) + \omega^2(t) y(t) = 0 \tag{A1}$$

We wish to ascertain the asymptotic behavior of the solutions in the limit of $\epsilon \to 0$. The formal WKB expansion is

$$y(t) \sim \exp\left[\epsilon^{-1} \sum_{n=0}^{\infty} \epsilon^n S_n(t)\right] \tag{A2}$$

The first and the second derivatives of $y(t)$ are

$$\dot{y}(t) \sim \epsilon^{-1} \left[\sum_{n=0}^{\infty} \epsilon^n \dot{S}_n(t)\right] \exp\left[\epsilon^{-1} \sum_{n=0}^{\infty} \epsilon^n S_n(t)\right] \tag{A3a}$$

$$\ddot{y}(t) \sim \left\{\epsilon^{-1} \sum_{n=0}^{\infty} \epsilon^n \ddot{S}_n(t) + \epsilon^{-2} \left[\sum_{n=0}^{\infty} \epsilon^n \dot{S}_n(t)\right]^2\right\} \exp\left[\epsilon^{-1} \sum_{n=0}^{\infty} \epsilon^n S_n(t)\right] \tag{A3b}$$

Substituting these into Eq. (A1) and gathering terms of order 1 and $\epsilon$, we obtain

$$\dot{S}_0^2 + \omega^2(t) = 0 \Rightarrow S_0 = \pm \int_0^t i\omega(s) ds \tag{A4a}$$

$$\ddot{S}_0 + 2\dot{S}_0 \dot{S}_1 = 0 \Rightarrow S_1 = -\frac{1}{4} \ln\{i\omega^2(t)\} \tag{A4b}$$

Therefore, the first-order WKB approximation is

$$y(t) \sim \mathrm{e}^{\epsilon^{-1} S_0 + S_1} \sim \omega^{-1/2}(t) \left\{A \cos\left[\epsilon^{-1} \int_0^t \omega(s)\, ds\right] + B \sin\left[\epsilon^{-1} \int_0^t \omega(s)\, ds\right]\right\} \tag{A5}$$

## APPENDIX B: CALCULATIONS FOR THE EAM POTENTIAL

The analytical expressions for the interaction potentials, the energy of the crystal, the force on each atom, the dynamical matrix of each atom, and the derivative of its trace are presented here. The potential energy based on the embedded-atom method is given as

$$V = \sum_{a=1}^{N} \left[F(\rho_a) + \frac{1}{2} \sum_b \phi(r_{ab})\right] \tag{B1}$$

where

$$\rho_a = \sum_b f(r_{ab}) \tag{B2}$$

is the electron density associated with atom $a$, $F$ is the embedding function, $\phi$ is the pairwise interaction term and $b \neq a$ denotes all the neighbors of atom $a$. The force at each atom is

$$\frac{\partial V}{\partial \boldsymbol{q}_a} = \sum_b \left\{[F'(\rho_a) + F'(\rho_b)] f'(r_{ab}) + \phi'(r_{ab})\right\} \frac{\boldsymbol{r}_{ab}}{r_{ab}} \tag{B3}$$

with

$$\boldsymbol{r}_{ab} = \boldsymbol{R}_a - \boldsymbol{R}_b$$

The trace of the stiffness matrix, $\boldsymbol{K}_a$ is of the form

$$\begin{aligned} \mathrm{Tr}\boldsymbol{K}_{aa} = &\sum_b \left[\phi''(r_{ab}) + 2\frac{\phi'(r_{ab})}{r_{ab}}\right] + \sum_b F''(\rho_b)[f'(r_{ab})]^2 + \sum_b F''(\rho_a) f'(r_{ab}) \left\{\sum_c f'(r_{ac}) \frac{\boldsymbol{r}_{ac}}{r_{ac}}\right\} \cdot \frac{\boldsymbol{r}_{ab}}{r_{ab}} \\ &+ \sum_b [F'(\rho_a) + F'(\rho_b)] \left[f''(r_{ab}) + 2\frac{f'(r_{ab})}{r_{ab}}\right] \end{aligned} \tag{B4a}$$

The gradient of the trace of the stiffness matrix, $\boldsymbol{K}_a$ is

$$\begin{aligned}\frac{\partial}{\partial \boldsymbol{u}_a}\mathrm{Tr}\,\boldsymbol{K}_a &= \sum_b \left[\phi'''(r_{ab}) + 2\frac{\phi''(r_{ab})}{r_{ab}} - 2\frac{\phi'(r_{ab})}{r_{ab}^2}\right]\frac{\boldsymbol{r}_{ab}}{r_{ab}} + \sum_b [F'(\rho_a) + F'(\rho_b)] \\ &\times \left[f'''(r_{ab}) + 2\frac{f''(r_{ab})}{r_{ab}} - 2\frac{f'(r_{ab})}{r_{ab}^2}\right]\frac{\boldsymbol{r}_{ab}}{r_{ab}} + \sum_b 2F''(\rho_b)\, f''(r_{ab}) f'(r_{ab})\frac{\boldsymbol{r}_{ab}}{r_{ab}} \\ &+ \sum_b F''(\rho_b) f'(r_{ab}) \left[f''(r_{ab}) + 2\frac{f'(r_{ab})}{r_{ab}}\right]\frac{\boldsymbol{r}_{ab}}{r_{ab}} + \sum_b F'''(\rho_b)[f'(r_{ab})]^3\frac{\boldsymbol{r}_{ab}}{r_{ab}} \\ &+ \sum_b F''(\rho_a)\left[f''(r_{ab}) + 2\frac{f'(r_{ab})}{r_{ab}}\right]\left\{\sum_c f'(r_{ac})\frac{\boldsymbol{r}_{ac}}{r_{ac}}\right\} \\ &+ \sum_b F'''(\rho_a)\left[\left\{\sum_c f'(r_{ac})\frac{\boldsymbol{r}_{ac}}{r_{ac}}\right\}\cdot\left\{\sum_c f'(r_{ac})\frac{\boldsymbol{r}_{ac}}{r_{ac}}\right\}\right]\left\{\sum_c f'(r_{ac})\frac{\boldsymbol{r}_{ac}}{r_{ac}}\right\} \\ &+ \sum_b 2F''(\rho_a)\left[\sum_c\left\{\frac{f'(r_{ac})}{r_{ac}}\delta + \left(f''(r_{ac}) - \frac{f'(r_{ac})}{r_{ac}}\right)\frac{1}{r_{ac}^2}\boldsymbol{r}_{ac}\otimes\boldsymbol{r}_{ac}\right\}\right]\left\{\sum_c f'(r_{ac})\frac{\boldsymbol{r}_{ac}}{r_{ac}}\right\}\end{aligned} \tag{B4b}$$

The gradient of the trace of the stiffness matrix, $\boldsymbol{K}_b$, $b$ being a neighbor of atom $a$, is

$$\begin{aligned}\frac{\partial}{\partial \boldsymbol{u}_a}\mathrm{Tr}\,\boldsymbol{K}_b &= \left[\phi'''(r_{ab}) + 2\frac{\phi''(r_{ab})}{r_{ab}} - 2\frac{\phi'(r_{ab})}{r_{ab}^2}\right]\frac{\boldsymbol{r}_{ab}}{r_{ab}} + [F'(\rho_a) + F'(\rho_b)]\left[f'''(r_{ab}) + 2\frac{f''(r_{ab})}{r_{ab}} - 2\frac{f'(r_{ab})}{r_{ab}^2}\right]\frac{\boldsymbol{r}_{ab}}{r_{ab}} \\ &+ 2F''(\rho_a)\, f''(r_{ab}) f'(r_{ab})\frac{\boldsymbol{r}_{ab}}{r_{ab}} + F''(\rho_b) f'(r_{ab})\left[\sum_c f''(r_{bc}) + 2\frac{f'(r_{bc})}{r_{bc}}\right]\frac{\boldsymbol{r}_{ab}}{r_{ab}} \\ &+ F'''(\rho_b) f'(r_{ab})\left[\left\{\sum_c f'(r_{bc})\frac{\boldsymbol{r}_{bc}}{r_{bc}}\right\}\cdot\left\{\sum_c f'(r_{bc})\frac{\boldsymbol{r}_{bc}}{r_{bc}}\right\}\right]\frac{\boldsymbol{r}_{ab}}{r_{ab}} \\ &+ 2F''(\rho_b)\left(f''(r_{ab}) - \frac{f'(r_{ab})}{r_{ab}}\right)\left[\left\{\sum_c f'(r_{bc})\frac{\boldsymbol{r}_{bc}}{r_{bc}}\right\}\cdot\frac{\boldsymbol{r}_{ab}}{r_{ab}}\right]\frac{\boldsymbol{r}_{ab}}{r_{ab}} + 2F''(\rho_b)\frac{f'(r_{ab})}{r_{ab}}\left\{\sum_c f'(r_{bc})\frac{\boldsymbol{r}_{bc}}{r_{bc}}\right\} \\ &+ F''(\rho_a)[f''(r_{ab}) + 2\frac{f'(r_{ab})}{r_{ab}}]\left\{\sum_c f'(r_{ac})\frac{\boldsymbol{r}_{ac}}{r_{ac}}\right\} + F'''(\rho_a)[f'(r_{ab})]^2\left\{\sum_c f'(r_{ac})\frac{\boldsymbol{r}_{ac}}{r_{ac}}\right\} \\ &+ \sum_d F'''(\rho_d) f'(r_{ad})[f'(r_{ab})]^2\frac{\boldsymbol{r}_{ad}}{r_{ad}} + \sum_d F''(\rho_d) f'(r_{ad})\left[f''(r_{bd}) + 2\frac{f'(r_{bd})}{r_{bd}}\right]\frac{\boldsymbol{r}_{ad}}{r_{ad}}\end{aligned} \tag{B5}$$

In the last two terms, $d$ represents those neighbors of $b$ that are also neighbors of $a$.